



Nonlinear interactions between unstable oscillatory modes in a cantilevered pipe conveying fluid

Kiyotaka Yamashita · Takahiro Yagyu · Hiroshi Yabuno

Received: 14 January 2019 / Accepted: 3 September 2019 / Published online: 11 September 2019
© Springer Nature B.V. 2019

Abstract Intense interest has been expressed in high-codimensional bifurcations and the nonlinear interactions between unstable modes. Nonlinear interactions between oscillatory modes can produce numerous complex motions. Such motions are caused by the double Hopf bifurcation. A cantilevered pipe conveying fluid is a typical non-conservative continuous system. When the flow velocity exceeds a critical value, a certain mode becomes unstable due to Hopf bifurcation which can be caused by the non-orthogonality of the eigenfunctions. Linear stability analyses have also revealed that another mode can experience an oscillatory instability as the flow velocity is increased further. Therefore, nonlinear interactions between two unstable modes become a problem. We focus on the double Hopf bifurcation of a pipe conveying fluid and investigate the nonlinear interactions between unstable second and third modes. We derive the amplitude equations governing the time evolution of the amplitudes of two unstable modes from a nonlinear nonself-adjoint partial differential equation and its boundary conditions. The theoretical results show that the self-excited planar pipe vibration can be produced either in the second or the third mode in a cer-

tain range of flow velocity, whereas the mixed-modal self-excited vibration is inhibited. Experiments were also conducted to verify the theoretical results. The theoretical results give a qualitatively good account of the typical features of double Hopf interactions in experiments.

Keywords Double Hopf bifurcation · Pipe conveying fluid · Nonlinear stability · Bifurcation

1 Introduction

Intense interest has been expressed in high-codimensional bifurcations. In non-conservative autonomous systems, nonlinear interactions between oscillatory modes can produce numerous complex motions. Such motions are caused by the double Hopf bifurcation [1,2]. The double Hopf bifurcation is a codimension two bifurcation. At the bifurcation point, the linearized system has two pairs of eigenvalues $\pm i\omega_m$ and $\pm i\omega_n$.

Chamara [3] theoretically investigated the double Hopf bifurcation of two airfoils elastically supported in a two-dimensional fluid flow. Each airfoil has two degrees of freedom (pitch and plunge), and the two airfoils are coupled only through the fluid. Shaw [4] theoretically investigated flexural vibrations of a rotating shaft taking into account internal damping. The reduced system obtained by Galerkin's method suggests the existence of a double Hopf bifurcation. They studied the qualitative behavior of the interactions of

K. Yamashita (✉) · T. Yagyu
Department of Mechanical Engineering, Fukui University
of Technology, 3-6-1 Gakuen, Fukui-shi, Fukui, Japan
e-mail: yamashita@fukui-ut.ac.jp

H. Yabuno
Graduate School of Systems and Information Engineering,
University of Tsukuba, 1-1-1 Ten-no-dai, Tsukuba Science,
Ibaraki, Japan

two unstable modes using the method of center manifold theory.

Such motions appear to widely exist in non-conservative continuous systems, which are subjected to the circulatory forces. We consider the self-excited pipe vibration as a typical example of self-excited vibrations which can be caused by the non-orthogonality of the eigenfunctions. Pipes conveying fluid have attracted interest because (i) they exhibit numerous complex motions, and (ii) they have emerged as a vehicle to test modern dynamical theory [5]. It is also well known that the system realizes self-excited lateral vibration of a beam subjected to the follower force. Moreover, experiments can be easily conducted to verify the theoretical results. Copeland and Moon [6] experimentally investigated the effect of an attached end mass on the post-flutter bifurcation phenomena and reported various three-dimensional motions. It is well known that the attached end mass enriches the dynamics of the pipe conveying fluid.

High-codimensional bifurcations are also attracting a great deal of attention in pipes. For cantilevered pipes with a spring support, Jin and Zou [7] focused on the doubly degenerate point, where coupled flutter and divergence bifurcations occur. In addition, three-dimensional motions of a cantilevered pipe that has rotational symmetry about the vertical axis have been an interesting phenomenon from the view-point of nonlinear dynamics [8,9]. When the flow velocity reaches the critical value, the linearized system has a double pair of complex conjugate eigenvalues $\omega_m = \omega_n$. The bifurcating three-dimensional motions are described with two amplitude equations and one phase equation. Moreover, Bajaj [10] investigated the symmetry-breaking effects on three-dimensional motions.

Another question is whether double Hopf bifurcation ($\omega_m \neq \omega_n$) can be produced or not. In the present paper, we focus on the double Hopf bifurcation ($\omega_m \neq \omega_n$) of the pipe conveying fluid. As a first step to investigate the double Hopf bifurcation in pipes, we consider the planar pipe vibration. In the present paper, we focus on the nonlinear interactions between unstable second and third modes. We first derive the two complex amplitude equations for two unstable modes. We conduct nonlinear analyses to clarify the nonlinear interactions between two unstable modes. In particular, we conduct experiments involving a silicone rubber pipe conveying water to qualitatively confirm the nonlinear features predicted by theoretical analyses.

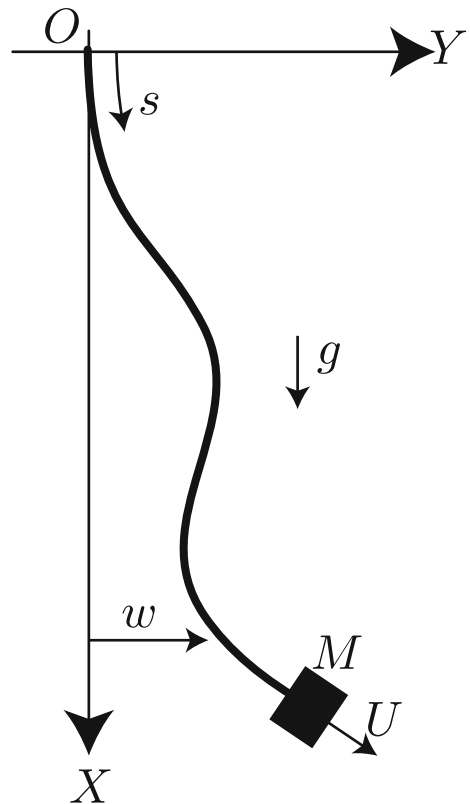


Fig. 1 Analytical model of planar self-excited pipe vibration

2 Basic equations

We briefly give some basic definitions and assumptions to derive the nonlinear governing equations presented in Yoshizawa [11]. We consider the planar pipe vibration in the $X - Y$ plane, as shown in Fig. 1. A pipe is hung vertically under the influence of gravity g . The upper end of the pipe is clamped, and the lower free end is fitted with lumped mass M . The pipe conveys an incompressible fluid of density ρ that discharges to the atmosphere from the free end. The flow in the pipe is assumed to be constant and one-dimensional, and the flow velocity U relative to the pipe motion is assumed to be parallel to the pipe centerline. In addition, the pipe is assumed to be a flexible and inextensible beam of length ℓ , flexural rigidity EI , mass per unit length m , and bore area S . The pipe is sufficiently long compared with its diameter.

Let w be the displacement along the pipe centerline in the Y direction. Displacement w is expressed as a function of the curvilinear coordinate s along the

pipe centerline and time t . Non-dimensionalization is achieved using the overall length of the pipe ℓ and the characteristic time $\sqrt{(m + \rho S)\ell^4/EI}$. The equation of pipe vibration in the $X - Y$ plane can be written with terms up to the third order of w^* in non-dimensional form [11]:

$$\begin{aligned} \ddot{w} + 2\sqrt{\beta}V\dot{w}' + V^2w'' - \gamma\{(\alpha + 1 - s)w'\}' + w'''' = \\ -w' \int_0^s \dot{w}'^2 ds - w' \int_0^s w' \ddot{w}' ds + w'' \int_s^1 \int_0^s \dot{w}'^2 ds ds \\ + \frac{1}{2}\ddot{w}w'^2 - w'' \int_s^1 \ddot{w}w' ds + w'' \int_s^1 \int_0^s w' \ddot{w}' ds ds \\ + \alpha w'' \int_0^1 \dot{w}'^2 ds + \alpha w'' \int_0^1 w' \ddot{w}' ds - \alpha w'' w'_1 \ddot{w}_1 \\ - \sqrt{\beta}Vw'^2 \dot{w}' - \frac{1}{2}V^2w'^2 w'' + \frac{1}{2}\gamma(1 - s)w'^2 w'' \\ - \frac{1}{2}\gamma w'' \int_s^1 w'^2 ds - \frac{1}{2}\alpha\gamma w'' w_1'^2 + \frac{1}{2}\alpha\gamma w'' w'^2 \\ - \frac{3}{2}w''^3 + \frac{1}{2}w'' w_1''^2 - 3w' w'' w''' - \frac{1}{2}w'^2 w'''' \end{aligned} \tag{1}$$

where $(\dot{\cdot})$ and $(\cdot)'$ denote the derivatives with respect to t and s , respectively. On the right-hand side of Eq. (1), the first through the ninth terms are associated with the inertial force, the tenth and the eleventh terms are associated with the Coriolis force and the centrifugal force, respectively, the twelfth through the fifteenth terms are associated with the gravitational force, and the remaining terms are associated with the flexural restoring force. The asterisks indicating the dimensionless variables are omitted in Eq. (1) and hereinafter. The subscript expression w_1 indicates w at $s = 1$. The boundary conditions for the pipe vibration in the $X - Y$ plane are also expressed as follows:

$$\begin{aligned} s = 0 : w = 0, \quad w' = 0, \\ s = 1 : w'' = 0, \\ w''' - \alpha\gamma w' - \alpha\ddot{w} = -\frac{1}{2}w''' w'^2 - w''^2 w' \\ + \alpha w' \int_0^1 \dot{w}'^2 ds + \alpha w' \int_0^1 w' \ddot{w}' ds - \frac{1}{2}\alpha\ddot{w}w'^2 \end{aligned} \tag{2}$$

Four dimensionless parameters are involved in Eqs. (1) and (2): flow velocity $V = \sqrt{\rho S l^2/EIU}$, the ratio of the lumped mass to the total mass $\alpha = M/(m + \rho S)l$, the ratio of the fluid mass to the total mass $\beta = \rho S/(m + \rho S)$, and the ratio of the gravitational force to the elastic force $\gamma = (m + \rho S)gl^3/EI$. In order to systematically derive the amplitude equations, we convert

the governing equations into vector form by defining $\mathbf{w} = (w \ \dot{w} + 2\sqrt{\beta}Vw')^t$. The governing equation of \mathbf{w} is expressed in vector form as follows:

$$\dot{\mathbf{w}} = L\mathbf{w} + N, \tag{3}$$

where

$$\begin{aligned} L = \begin{pmatrix} -2\sqrt{\beta}V(\cdot)' & 1 \\ L_{21} & 0 \end{pmatrix}, \quad N = \begin{pmatrix} 0 \\ n \end{pmatrix}, \\ L_{21} = -(\cdot)'''' + \gamma\{(\alpha + 1 - s)(\cdot)'\}' - V^2(\cdot)'' \end{aligned} \tag{4}$$

The boundary conditions associated with \mathbf{w} are as follows:

$$s = 0 : B_1\mathbf{w} = 0, \quad s = 1 : B_2\dot{\mathbf{w}} = B_3\mathbf{w} - N_b, \tag{5}$$

where

$$\begin{aligned} B_1 = \begin{pmatrix} 1 & 0 \\ (\cdot)' & 0 \end{pmatrix}, \quad B_2 = \begin{pmatrix} 0 & 0 \\ -2\sqrt{\beta}V\alpha(\cdot)' & \alpha \end{pmatrix}, \\ B_3 = \begin{pmatrix} (\cdot)'' & 0 \\ (\cdot)''' - \alpha\gamma(\cdot)' & 0 \end{pmatrix}, \quad N_b = \begin{pmatrix} 0 \\ b \end{pmatrix} \end{aligned} \tag{6}$$

and n and b in Eqs. (4) and (6) are expressed as nonlinear polynomials respect to w describing Eqs. (1) and (2).

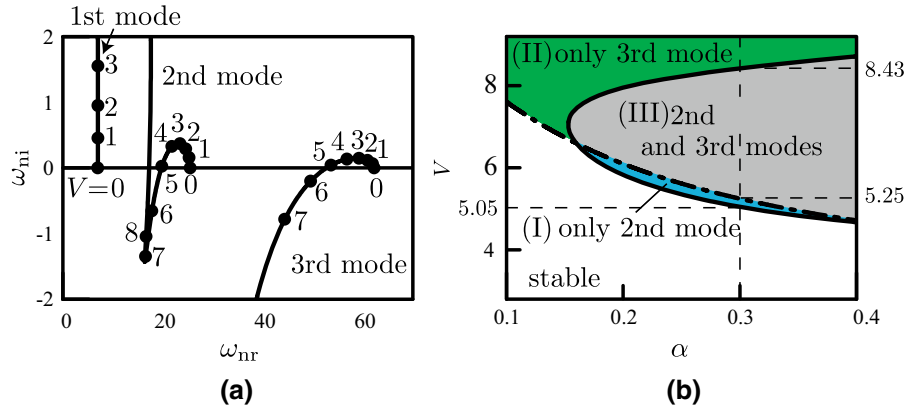
3 Linear stability and adjoint function

3.1 Unstable regions

In this section, the linear stability analysis of the lateral vibration of a pipe with an end mass is briefly described to determine the vibration modes and the linear complex natural frequencies as a function of V . Moreover, to estimate the existence of the double Hopf bifurcations, parameter regions where two distinct eigenmodes simultaneously become unstable are examined.

We disregard the nonlinear terms in Eqs. (3) and (5) in order to investigate the linear stability. After letting $\mathbf{w} = \mathbf{q}_n e^{\lambda_n t}$ and $\mathbf{q}_n(s) = (\Phi_{n1}(s) \ \Phi_{n2}(s))^t$, ($n = 1, 2, \dots$), and substituting these terms into Eqs. (3) and (5), we construct the eigenvalue problems. Calculations of the linear eigenvalues and eigenmodes for the lowest three modes, which are described in a power series of s that satisfies the governing equation and the boundary conditions, are conducted. The n th eigenvalue λ_n , being the root of the complex characteristic equation, which is symbolically described by $f(\lambda_n; V, \alpha, \beta, \gamma) = 0$, can be found numerically. Here, λ_n

Fig. 2 Linear stability ($\beta = 0.25$ and $\gamma = 32.8$). **a** Eigenvalues λ_n as a function of the flow velocity V for the lowest three modes ($\alpha = 0.3$), and **b** unstable regions on $\alpha - V$ plane: (I) second mode is unstable ($\omega_{2i} < 0$), (II) third mode is unstable ($\omega_{3i} < 0$), and (III) second and third modes are unstable ($\omega_{2i} < 0, \omega_{3i} < 0$)



is equal to $i(\omega_{nr} + i\omega_{ni})$, where ω_{nr} is the natural frequency and ω_{ni} corresponds to the damping ratio.

In the case of $\alpha = 0.3, \beta = 0.25$ and $\gamma = 32.8$, ω_{nr} and ω_{ni} ($n = 1, 2, 3$) are shown as a function of V in Fig. 2a. The first mode is stable because $\omega_{1i} > 0$. When V increases, ω_{2i} becomes negative at $V = 5.05$, and the system becomes unstable by Hopf bifurcation. Above $V = 5.25$, ω_{3i} also becomes negative. Then, another Hopf bifurcation occurs. For $8.43 < V$, ω_{2i} becomes positive again. Therefore, for $5.25 < V < 8.43$, both ω_{2i} and ω_{3i} are negative and the Hopf–Hopf interactions become a problem. The given parameter values used in the numerical examples henceforward are equal to the experimental values in Sect. 5.

We then calculate the effect of additional mass α on the unstable regions for the self-excited vibrations. Figure 2b shows the unstable regions on the $\alpha - V$ plane. The area enclosed by the solid line indicates the region in which ω_{2i} is negative, and the area above the dash-dotted line indicates the region where ω_{3i} is negative. The unstable region can be divided into three regions: (I) $\omega_{2i} < 0, \omega_{3i} > 0$, (II) $\omega_{2i} > 0, \omega_{3i} < 0$, and (III) $\omega_{2i} < 0, \omega_{3i} < 0$. At the points where the solid line and the dash-dotted line intersect, the second and the third modes become unstable simultaneously and the system experiences double Hopf bifurcation. Figure 2b shows that the second and the third modes become unstable almost simultaneously for a certain range of parameters.

3.2 Adjoint function

The motions of the pipe are governed by the nonself-adjoint partial differential equation and the boundary

conditions. Then, the eigenfunctions in the pipe do not belong to the system of orthogonal functions. Therefore, in order to capture the evolution of the finite amplitudes, we need to project the system nonlinearity to the unstable eigenspaces using the adjoint functions $\mathbf{q}_n^* = (\psi_{n1} \ \psi_{n2})^t$ ($n = 1, 2, 3, \dots$). The adjoint functions \mathbf{q}_n^* ($n = 1, 2, 3, \dots$) are described as follows:

$$\lambda_n \begin{pmatrix} \psi_{1n} \\ \psi_{2n} \end{pmatrix} = L^* \begin{pmatrix} \psi_{1n} \\ \psi_{2n} \end{pmatrix}, \tag{7}$$

where

$$L^* = \begin{pmatrix} 2\sqrt{\beta}V(\cdot)' & L_{12}^* \\ 1 & 0 \end{pmatrix}.$$

$$s = 0 : \psi_{2n} = 0, \ \psi_{2n}' = 0,$$

$$s = 1 : \psi_{2n}'' = -V^2\psi_{2n},$$

$$\psi_{2n}''' = 2\sqrt{\beta}V\psi_{1n} + \alpha\gamma\psi_{2n}' - V^2\psi_{2n}' + \alpha\lambda_n\psi_{1n}, \tag{8}$$

$$\text{where } L_{12}^* = -(\cdot)'''' + \gamma \left\{ (\alpha + 1 - s)(\cdot)' \right\}' - V^2(\cdot)''.$$

We also calculate the adjoint function \mathbf{q}^* , which is described in a power series of s that satisfies Eqs. (7) and (8).

4 Nonlinear interactions between two unstable modes

4.1 Amplitude equations

We can express the solution space \mathbf{Z} as $\mathbf{Z} = \mathbf{X} \oplus \mathbf{M}$. Then, \mathbf{X} is spanned by two unstable eigenvectors \mathbf{q}_2 and \mathbf{q}_3 , and \mathbf{M} is the complementary subspace of \mathbf{X} . Therefore, \mathbf{w} is expressed as follows:

$$\mathbf{w} = C_2\mathbf{q}_2 + C_3\mathbf{q}_3 + \mathbf{y} + \text{c.c.}, \tag{9}$$

where \mathbf{y} is the element of \mathbf{M} and c.c. denotes the complex conjugate of the preceding terms. In addition, C_2 is the complex amplitude of vibration in the second mode, and C_3 is that in the third mode.

As in the previous study [12], using the adjoint function $\mathbf{q}_2 = (\psi_{21}, \psi_{22})^t$ and the projection $P\mathbf{x} = \langle \mathbf{x}, \bar{\mathbf{q}}_2^* \rangle = \left\{ \int_0^1 \mathbf{x} \cdot \bar{\mathbf{q}}_2^* ds + \alpha \mathbf{x}(1) \cdot \bar{\mathbf{q}}_2^*(1) - 2\sqrt{\beta}V\alpha x_1'(1)\psi_{22}(1) \right\} \mathbf{q}_2$, where $\mathbf{x} = (x_1, x_2)^t$ and (\cdot) indicates the inner product, we can project the nonlinear governing equation on the eigenspace spanned by \mathbf{q}_2 . Producing the terms proportional to $e^{i\omega_{2r}t}$ from the projected governing equation, the following evolutionary amplitude equation can be obtained.

$$\dot{A} = -\omega_{2i}A + \xi_1 A^2 \bar{A} + \xi_2 AB\bar{B}, \tag{10}$$

where $C_2 = Ae^{i\omega_{2r}t}$. The evolutionary amplitude equation of complex amplitude B can be obtained in the manner described above:

$$\dot{B} = -\omega_{3i}B + \xi_3 B^2 \bar{B} + \xi_4 BA\bar{A}, \tag{11}$$

where $C_3 = Be^{i\omega_{3r}t}$ and $\xi_n = \xi_{nr} + i\xi_{ni}$ ($n = 1, \dots, 4$) in Eqs. (10) and (11) are the complex values determined by α, β, γ and V . Letting $A = a \exp(i\phi)/2$ and $B = b \exp(i\psi)/2$ in Eqs. (10) and (11), where a, b, ϕ , and ψ are real, and separating the real and imaginary parts, we obtain

$$\dot{a} = \left(-\omega_{2i} + \frac{\xi_{1r}}{4}a^2 + \frac{\xi_{2r}}{4}b^2 \right) a, \tag{12}$$

$$\dot{b} = \left(-\omega_{3i} + \frac{\xi_{3r}}{4}b^2 + \frac{\xi_{4r}}{4}a^2 \right) b, \tag{13}$$

$$a\dot{\phi} = \left(\frac{\xi_{1i}}{4}a^2 + \frac{\xi_{2i}}{4}b^2 \right) a, \tag{14}$$

$$b\dot{\psi} = \left(\frac{\xi_{3i}}{4}b^2 + \frac{\xi_{4i}}{4}a^2 \right) b. \tag{15}$$

Since ω_{3r}/ω_{2r} is irrational, the equations of the amplitudes and the phases are not coupled. Therefore, in order to study the bifurcating pipe motions, it is sufficient to consider only Eqs. (12) and (13). Equations (12) and (13) are in the same form as a normal form of the pure imaginary pairs of eigenvalues without resonance [13]. Equations (14) and (15) give the nonlinear correction values for the linear eigenfrequencies.

We explain the roles of the nonlinear terms in Eq. (12). In the case of single-mode flutter ($b = 0$), the steady-state amplitude of a_s is determined when the first term on the right-hand side of this equation balances the second term. Within the limits of our examinations, both ξ_{2r} and ξ_{4r} are negative. Then, in the case

of $b \neq 0$, the third term acts as a damping term and suppresses a . Similar relationships are found in Eq. (13).

The horizontal displacement w of the pipe is expressed as follows:

$$w = a|\Phi_{21}| \cos(\omega_{2r}t + \phi + \angle\Phi_{21}) + b|\Phi_{31}| \cos(\omega_{3r}t + \psi + \angle\Phi_{31}), \tag{16}$$

where $|\Phi_{n1}|$ and $\angle\Phi_{n1}$, ($n = 2, 3$) are the magnitude and argument of Φ_{n1} , respectively.

4.2 Steady-state solutions of amplitude equations

The steady-state solutions a_s and b_s are obtained by substituting $\dot{a} = \dot{b} = 0$ into Eqs. (12) and (13). We obtain the following four steady-state solutions (a_s, b_s): (i) trivial solution, (ii) vibration in the second mode, (iii) vibration in the third mode, and (iv) mixed-modal self-excited vibration.

$$(i) : (a_s, b_s) = (0, 0), \tag{17}$$

$$(ii) : (a_s, b_s) = \left(2\sqrt{\frac{\omega_{2i}}{\xi_{1r}}}, 0 \right), \tag{18}$$

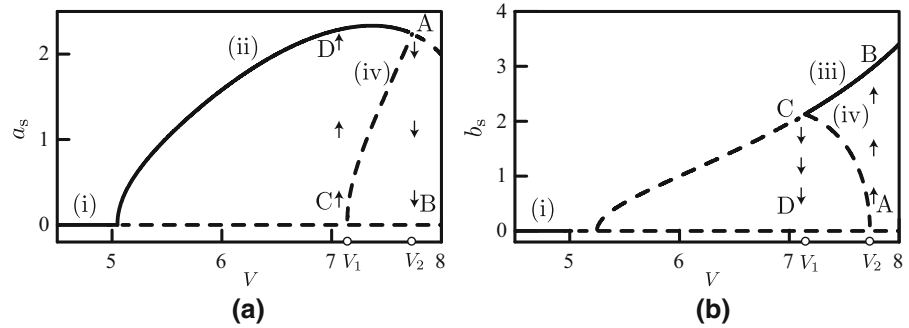
$$(iii) : (a_s, b_s) = \left(0, 2\sqrt{\frac{\omega_{3i}}{\xi_{3r}}} \right), \tag{19}$$

$$(iv) : (a_s, b_s) = \left(2\sqrt{\frac{(\omega_{2i}\xi_{3r} - \omega_{3i}\xi_{2r})}{(\xi_{1r}\xi_{3r} - \xi_{2r}\xi_{4r})}}, 2\sqrt{\frac{(\omega_{2i}\xi_{4r} - \omega_{3i}\xi_{1r})}{(\xi_{2r}\xi_{4r} - \xi_{1r}\xi_{3r})}} \right). \tag{20}$$

In order to determine the stability of these steady-state solutions, we assume $a = a_s + a_d(t)$ and $b = b_s + b_d(t)$. Substituting these equations into Eqs. (12) and (13) and keeping only the linear terms in a_d and b_d , we obtain the governing equations of infinitesimal disturbances a_d and b_d . We can determine the stability of steady states a_s and b_s by calculating the eigenvalues of a coefficient matrix in the governing equations of a_d and b_d .

We examine the effects of flow velocity V on the steady-state solutions a_s and b_s . The bifurcation diagrams of a_s and b_s are shown in Fig. 3. In these figures, the solid and broken lines correspond to stable and unstable steady-state solutions, respectively. The trivial solution described by (i) is stable for $V < V_{cr} = 5.05$, above which ω_{2i} becomes negative. At $V = V_{cr}$, the straight position of the pipe experiences a supercritical Hopf bifurcation. Consequently, the trivial solution

Fig. 3 Bifurcation diagrams of the steady-state amplitudes a_s and b_s under the influence of double Hopf bifurcation ($\alpha = 0.3$, $\beta = 0.25$ and $\gamma = 32.8$). Solid line: stable steady-state amplitudes, broken line: unstable steady-state amplitudes



becomes unstable, and a new branch of steady-state solutions, described by (ii) in Fig. 3, emerges from this bifurcation point. The value of a_s on branch (ii) is identical to the amplitude of the self-excited vibration in only the second mode. As V increases, the self-excited vibration in the second mode (ii) continues, although ω_{3i} becomes negative above $V = 5.25$. As V increases beyond $V_2 = 7.73$, steady-state solutions (ii) become unstable and a_s jumps from A to zero and b_s from zero to B. This steady-state solution corresponds to the self-excited vibration in the third mode (iii). Here, V_2 is the upper limit of V at which the self-excited vibration in the second mode (ii) occurs.

When V decreases slowly from a large value above $V_2 = 7.73$, b_s follows the curve through B and C. When V decreases below $V_1 = 7.14$, a_s jumps from zero to D and b_s decreases from C to zero. Here, V_1 is the lower limit of V at which the self-excited vibration in the third mode (iii) occurs. For the further decrease in V , the self-excited vibration in the second mode (ii) continues down to $V = V_{cr} = 5.05$. Therefore, in the case of $7.14 < V < 7.73$, there are two stable steady-state solutions (ii) and (iii). Moreover, the unstable solutions described by (iv) in Fig. 3 appear in this region. The velocity region $7.14 < V < 7.73$ is much smaller than the linear estimation $5.25 < V < 8.43$.

The qualitative classification of Eqs. (12) and (13) is given with all generality [13]. The pipe motions in Fig. 3 can be classified as shown in Fig. 4a. Figure 4b shows the variation of the nonlinear coefficients ξ_{2r} and ξ_{4r} as a function of α at $V = V_{cr}$. According to the considerations of Eqs. (12) and (13), the nonlinear terms can be deduced to restrict the evolution of amplitudes because of $\xi_{2r} < 0$ and $\xi_{4r} < 0$.

We numerically integrate Eqs. (12) and (13). Figure 5a–d show the flow around the steady-state solutions. The \bullet and \circ denote the stable and unstable steady-

state solutions, respectively. The arrows indicate the directions of time evolutions of a and b . When the flow velocity V increases above the critical flow velocity $V_{cr} = 5.05$, all flows settle at the only stable solution (ii) in Figs. 5a ($V = 5.1$) and b ($V = 7.0$) after a sufficient time. Figure 5c shows the flow for $7.14 < V = 7.50 < 7.73$. A non-trivial unstable solution indicates the unstable steady-state solution (iv). Here, E^s and E^u indicate the stable and unstable eigenvectors, respectively, for this non-trivial unstable solution. This point is a saddle point that separates regions of the above-mentioned qualitatively different motions. We numerically integrate Eqs. (12) and (13) by giving two initial condition (i) $t = 0 : a = 0.1, b = 0.1$ and (ii) $t = 0 : a = 0.1, b = 0.2$. Figure 5e and f shows the time histories of a and b for $V = 7.5$. Figure 5e shows that a converges to the steady-state amplitude (ii) in Fig. 3, whereas the growth of b is suppressed and b approaches zero. Figure 5f shows that b converges to the steady-state amplitude (iii) in Fig. 3, and a approaches zero. Therefore, the self-excited planar pipe vibration may be produced either in the second or the third mode, depending on the initial conditions. When V increases further, all flows settle at the only stable solution (iii) in Fig. 5d ($V = 7.8$) after a sufficient time.

Figure 6 shows the bifurcation set on the α – V plane. The post-flutter region is divided into three regions: (I) only steady-state solution (ii) is stable, (II) only steady-state solution (iii) is stable, and (III) steady-state solutions (ii) and (iii) are stable. The dash–dotted line indicates the linear stability boundaries for the second mode ($\omega_{2i} = 0$). Two solid lines also indicate V_1 over which steady-state solution (iii) is stable and V_2 below which steady-state solution (ii) is stable. Compared with the linear unstable region shown in Fig. 2b, region (III) becomes much smaller because of the nonlinear modal

Fig. 4 Classification of the pipe motions in the ω_{2i} - ω_{3i} plane. **a** Phase portraits in the ω_{2i} - ω_{3i} plane, and **b** Variation of the nonlinear coefficients ξ_{2r} and ξ_{4r} as a function of α at $V = V_{cr}$

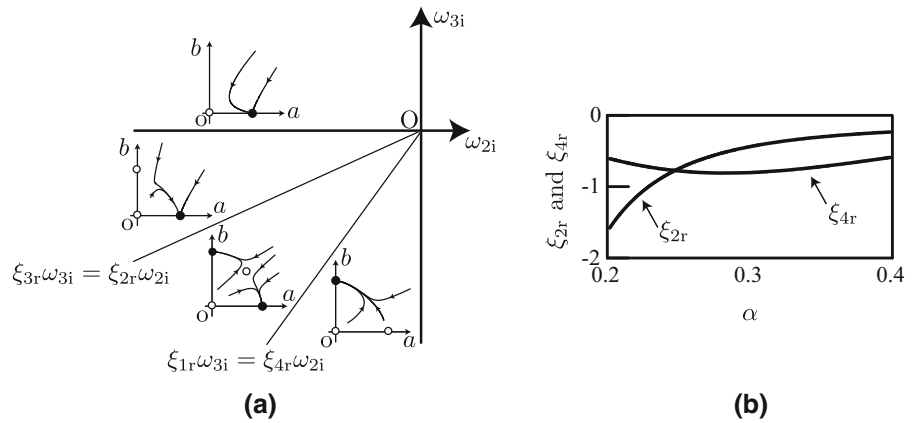
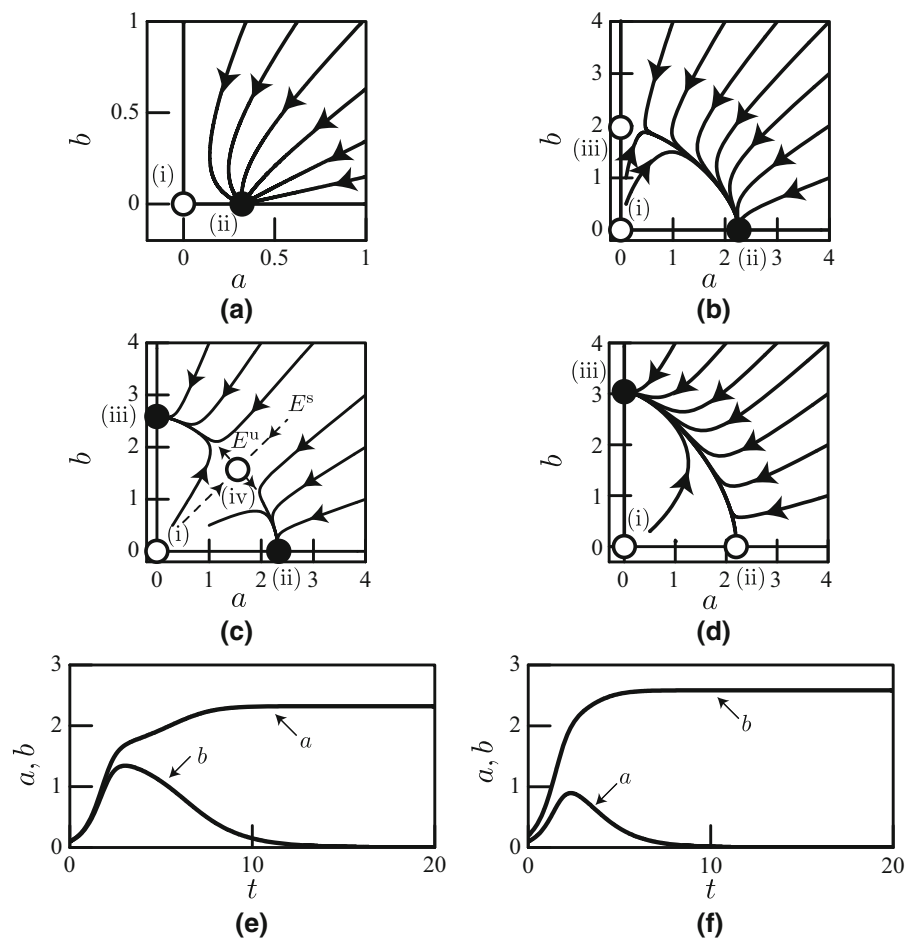


Fig. 5 Flow around the steady-state solutions: **a** $V = 5.1$, **b** $V = 7.0$, **c** $V = 7.5$, and **d** $V = 7.8$. All flows settle at stable solution (ii) or (iii) in Fig. 3. Here, E^s and E^u represents the stable and unstable eigenvectors at non-trivial unstable solution (iv). \bullet : stable steady-state solution, \circ : unstable steady-state solution. Time histories of a and b for $V = 7.5$: **e** initiated $(a, b) = (0.1, 0.1)$ and **f** $(0.1, 0.2)$



interactions. When α increases, self-excited vibrations in the second mode become dominant and widely suppress the growth of self-excited vibrations in the third mode.

5 Experiments

5.1 Experimental apparatus

We provide an outline of our experimental apparatus and procedures. We used a silicone rubber pipe with an

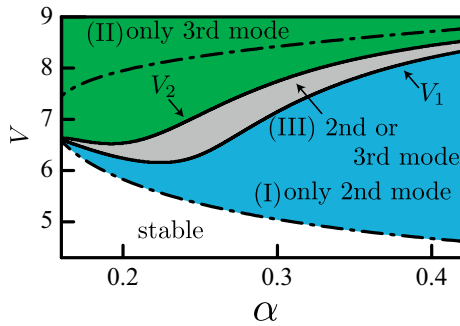


Fig. 6 Bifurcation set on the α - V plane: (I) self-excited vibration in second mode, (II) in third mode and (III) in second mode or in third mode. Dash-dotted lines indicate the linear stability $\omega_{2i} = 0$

external diameter of 12 mm and an internal diameter of 7 mm. The pipe had a circular cross section, and the pipe motion was not restricted by any constraints. The pipe had an overall length of 470 mm. It was molded silicone rubber to maintain the static equilibrium state to be as straight as possible. The flowing fluid was water. The pipe was clamped at the upper end and was fitted with a mass M at the other end. The additional mass was a brass ring with a mass of 16.3 g ($\alpha = 0.30$).

The schematic experimental apparatus is shown in Fig. 7. This experimental system was similar to that

used in a previous study [12]. The volume of flowing water was continuously measured by a Coriolis flow sensor (KEYENCE FD-SS20A). There are valves in the watercourse that allowed the mean flow velocity to be changed by the amount that the valve was opened. The pipe motions in 3D space were sensed by a movement analysis system in real time (OKK Inc., Quick Mag System). The system enabled us to conduct non-contact measurements of pipe motions in 3D space at a rate of 120 times per second. The measurements of pipe motions were continuously conducted, and the data were stored in a computer. The lateral displacements w of the pipe were sensed by the system at $s = 329$ mm (non-dimensional expression $s^* = 0.7$).

The experimental parameter values ($\alpha = 0.3$, $\beta = 0.25$, $\gamma = 32.8$), where the double Hopf bifurcation was expected, were estimated through linear stability analyses and preparatory experiments. The mean flow velocity was slowly increased from 3.0 m/s in the following quasi-static manner. Once the amplitude of the pipe vibration settled at a constant value, the image processing system took 120 measured values per second continuously for 140 s. After that, the mean flow velocity was slightly increased so that we could exclude the irregular variations caused by disturbances as much as

Fig. 7 Experimental setup and measurement system

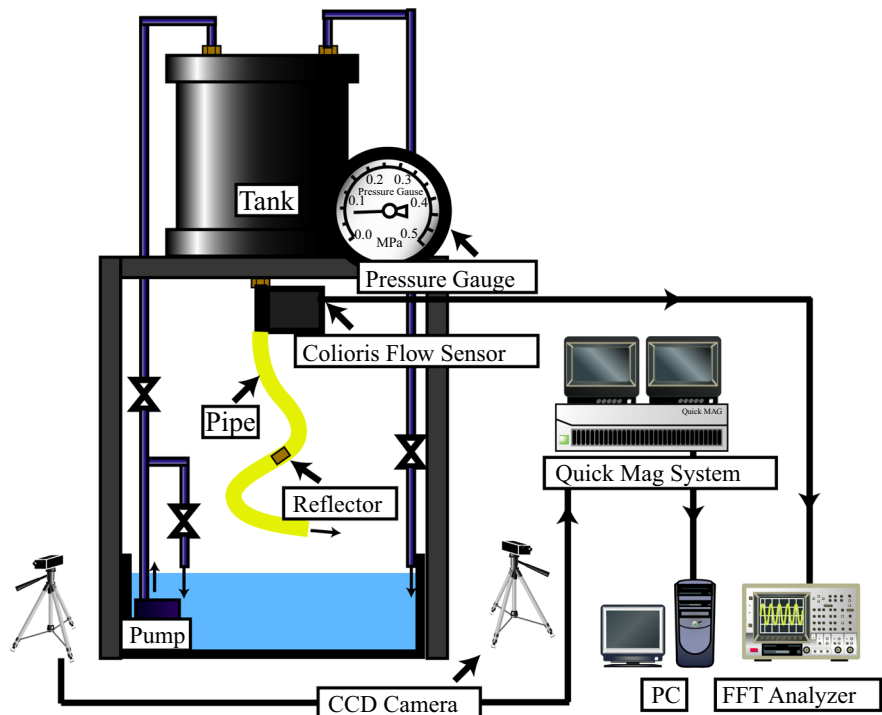
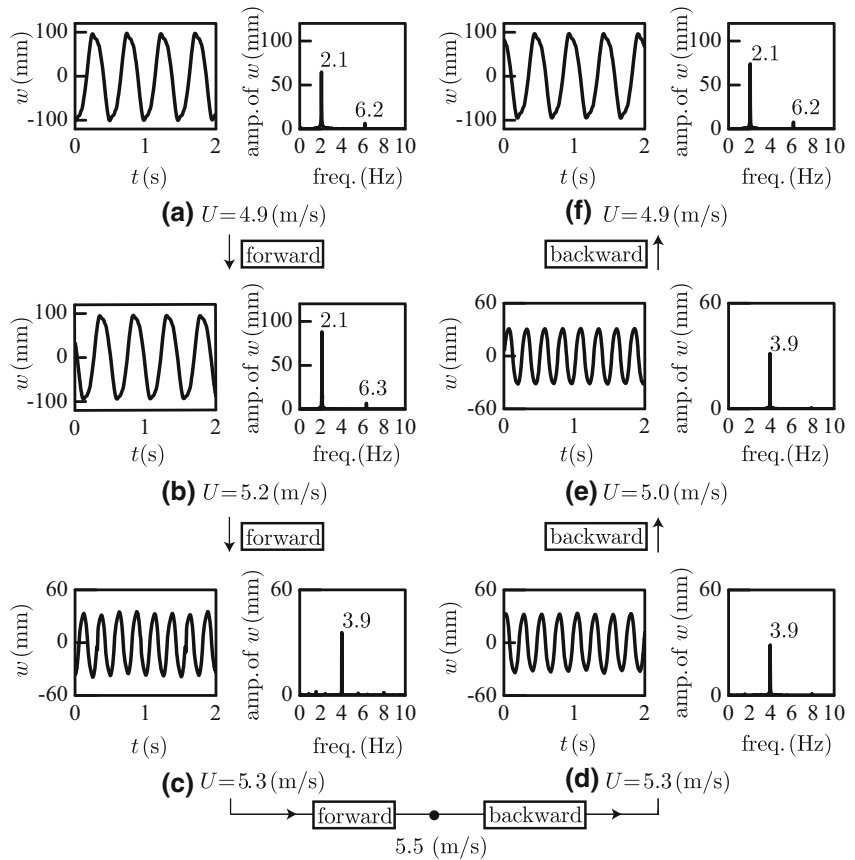


Fig. 8 Time histories of w and its frequency spectrum: **a** $U = 4.9$ m/s, **b** $U = 5.2$ m/s, **c** $U = 5.3$ m/s, **d** $U = 5.3$ m/s, **e** $U = 5.0$ m/s, and **f** $U = 4.9$ m/s



possible. We repeated this procedure. After the flow velocity reached 5.5 m/s, the flow velocity was slowly decreased to 3.0 m/s in the same manner.

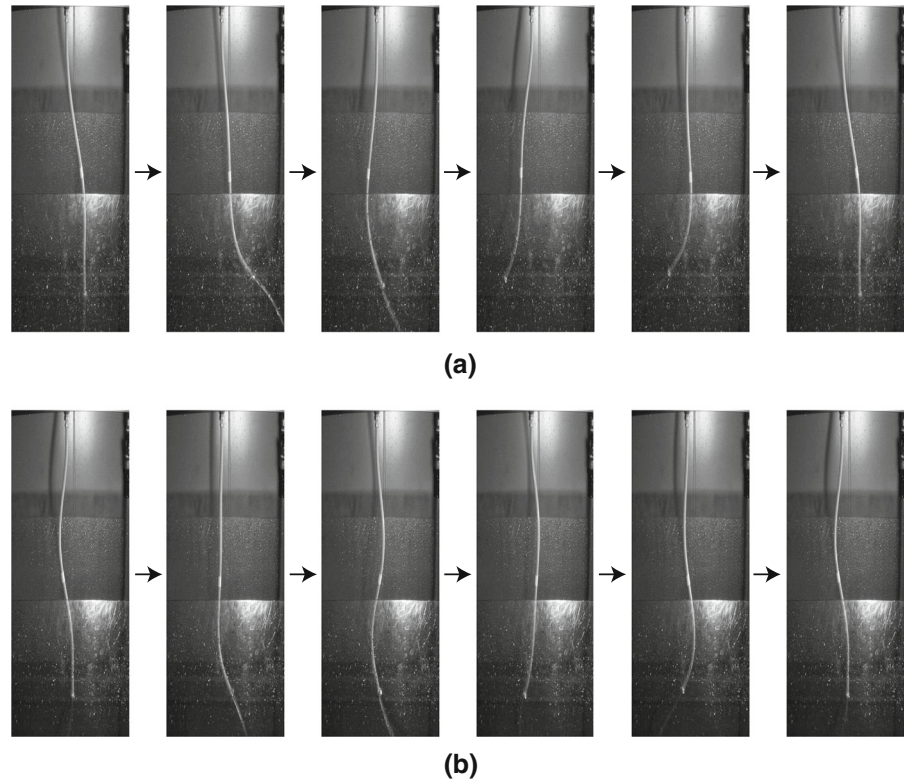
5.2 Experimental results

When U reached 3.6 m/s, the planar self-excited pipe vibration in the second mode occurred. The critical flow velocity $U = U_{cr}$ in the second mode was 3.6 m/s ($V_{cr} = 4.8$). This value was 95% of the theoretical value. Figure 8 shows a series of time histories of w and its frequency spectrum. As shown in Fig. 8a, in the case of $U = 4.9$ m/s, the distinguished frequency component of w was 2.1 Hz, which corresponded to the natural frequency of the second mode. The small superharmonic component 6.2 Hz is three times the distinguished frequency 2.1 Hz. Under different initial conditions at $U = 4.9$ m/s, we could not observe qualitatively different steady-state pipe vibrations. Figure 9a shows a series of photographs showing the self-excited pipe vibration in the second mode during a period at

$U = 5.2$ m/s. The self-excited vibration in the second mode was observed below $U = 5.2$ m/s, as shown in Fig. 8b. When U reached 5.3 m/s, the pipe vibration changes suddenly to planar self-excited pipe vibration in the third mode as shown in Fig. 8c. The distinguished frequency component of w was 3.9 Hz, which corresponded to the natural frequency of the third mode. Over $U = 5.3$ m/s, we could not observe qualitatively different steady-state pipe vibrations under different initial conditions.

When U decreased from 5.5 m/s, the self-excited vibration in the third mode could be observed above $U = 5.0$ m/s, as shown in Fig. 8d and e. Figure 9b shows a series of photographs showing the self-excited pipe vibration in the third mode during a period at $U = 5.2$ m/s. When U reached 4.9 m/s, the pipe vibration changes suddenly to planar self-excited pipe vibration in the second mode as shown in Fig. 8f. Therefore, from $U = 5.0$ m/s (non-dimensional value $V = 6.6$) to $U = 5.2$ m/s ($V = 6.9$), self-excited vibrations in the second or third modes could be produced. This region

Fig. 9 Series of photographs showing the self-excited pipe vibration at $U = 5.2$ m/s. **a** Self-excited vibration in the second mode, **b** self-excited vibration in the third mode



in the experiments was slightly smaller than the theoretical results (dimensionless form $V_2 - V_1 = 0.6$). The self-excited vibration in the second mode could not be observed below the critical flow velocity $U_{cr} = 3.6$ m/s. The theoretical results give a qualitative good account of typical features of double Hopf interactions in the experiments.

6 Conclusion

In this paper, we have studied the nonlinear stabilities of planar self-excited pipe vibrations corresponding to eigenvalues of two distinct modes almost simultaneously crossing the imaginary axis. Nonlinear analyses are conducted to clarify the nonlinear interactions between unstable second and third modes.

We first derive the complex amplitude equations from a nonlinear nonself-adjoint partial differential equation and its boundary conditions. Since the ratio of the natural frequencies ω_{3r}/ω_{2r} is irrational, the equations governing the bifurcating pipe motions are described by the amplitudes of two unstable modes. From the bifurcation analysis of the amplitude equa-

tions, we clarify that the self-excited pipe vibration in the second mode, which has the lowest critical flow velocity, suppresses the amplitude of the third mode. The self-excited vibration in the second mode can last even after the flow velocity increases slowly above the critical value at which the damping ratio of the third mode becomes negative and changes to the self-excited vibration in the third mode when the flow velocity increases further. In the case of slowly decreasing flow velocity, the self-excited vibration in the third mode can last below the upper limit of the flow velocity for the second mode vibration. Therefore, in a certain range of flow velocity, self-excited planar pipe vibrations can be produced either in the second or the third mode, depending on the initial conditions.

Finally, experiments were conducted to verify the theoretical results. As predicted in the theoretical analysis, we confirmed that self-excited vibrations in the second or third modes can be produced within a certain range of flow velocity. The theoretical results give a qualitatively good account of the typical features of double Hopf interactions in the experiments.

Acknowledgements The authors thank Professor Emeritus M. Yoshizawa for the useful discussions.

Funding This work does not receive any funding.

Compliance with ethical standards

Conflict of interest The authors declare no conflict of interest associated with this manuscript.

Human participants and animals This paper does not include human participants and animals.

Appendix A

Here, we outline the derivation of Eq. (1). We consider the small elements of the pipe and the fluid as shown in Fig. 10. We assume that the static equilibrium state in Fig. 10a is deformed as shown in Fig. 10b, where u is the displacement in the X direction. Applying a Newtonian derivation, we obtain the following equation:

$$(m + \rho S)(\ddot{u} + \ddot{v}j) = T't + Tt' + Q'n + Qn' + (m + \rho S)gi - 2\rho SV\dot{\theta}n - P'St - PSt' - \rho SV^2t', \quad (21)$$

Fig. 10 Geometric relationship on the small elements δs for **a** static equilibrium, **b** deformed element

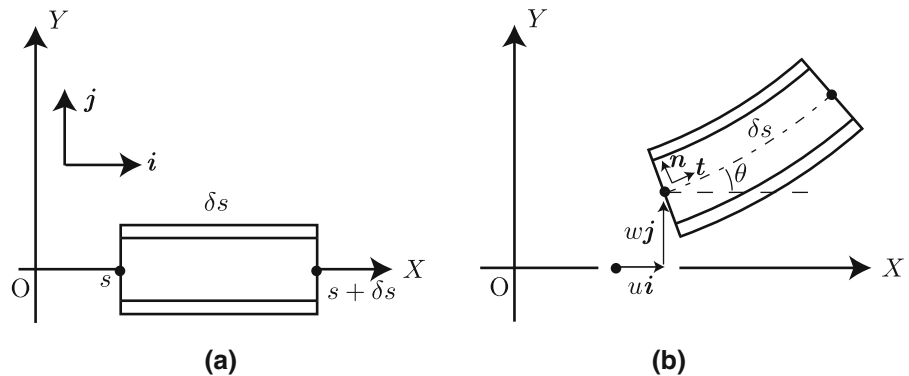
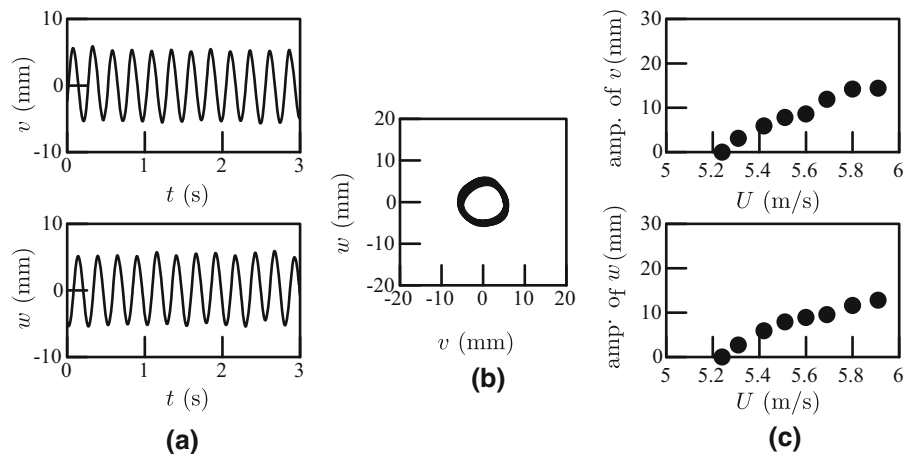


Fig. 11 Rotating motion of the self-excited pipe vibration in the third mode. **a** Time histories of v and w ($U = 5.3$ m/s, $M = 5.4$ g), **b** Pipe motion in the horizontal plane ($U = 5.3$ m/s, $M = 5.4$ g), **c** Bifurcation diagram of the rotating pipe motion in the third mode



where i and j are fundamental vectors. t is a unit vector in the direction of the neutral axis, and n is a unit vector perpendicular to t . θ is the angle between the neutral axis and the X axis. T , Q , and P denote the axial tension, the shearing force, and the pressure. Using $Q = -EI\theta''$, an inextensible condition and geometric relationships, this equation can be written in terms of w and we obtain Eq. (1).

Appendix B

Here, we briefly discuss the non-planar rotating pipe vibration in the third mode. In the case of $M = 5.4$ g ($\alpha = 0.1$), non-planar rotating motions are produced for $U > 5.3$ m/s. Figure 11a shows the time histories of displacements v and w parallel to the two perpendicular axes intersecting each other in the horizontal plane. The dominant frequency of the pipe vibration is 3.9 Hz which corresponds to the third mode natural frequency. The phase difference between v and w is almost $\pi/2$ and the pipe experiences rotating motion as shown in

Fig. 11b. Figure 11c shows the bifurcation diagram of the rotating pipe motion. We increase U from 5.3 m/s through 6.0 m/s. In this region, the rotating pipe motion is the only stable steady-state motion and we did not observe modal interactions.

References

1. Ding, Y., Jiang, W., Yu, P.: Double Hopf bifurcation in delayed van der pol-duffing equation. *Int. J. Bifurc. Chaos* **23**, 1350014-1–15 (2013)
2. Revel, G., Alonso, D.D., Muiola, J.L.: Interactions between oscillatory modes near a 2:3 resonant hopf-hopf bifurcation. *Chaos* **20**, 043106-1–8 (2010)
3. Chamara, P.A., Collier, B.D.: A study of double flutter. *J. Fluids Struct.* **19**, 863–879 (2004)
4. Shaw, J., Shaw, S.W.: Instabilities and bifurcations in a rotating shaft. *J. Sound Vib.* **132**, 227–244 (1989)
5. Paidoussis, M.P.: *Fluid-Structure Interactions: Slender Structures and Axial Flow*, vol. 1, pp. 1–3. Academic Press, London (1998)
6. Copeland, G.S., Moon, F.C.: Chaotic flow-induced vibration of a flexible tube with end mass. *J. Fluids Struct.* **6**, 705–718 (1992)
7. Jin, J.D., Zou, G.S.: Bifurcations and chaotic motions in the autonomous system of a restrained pipe conveying fluid. *J. Sound Vib.* **260**, 783–805 (2003)
8. Bajaj, A.K., Sethna, P.R.: Flow induced bifurcations to three-dimensional oscillatory motions in continuous tubes. *SIAM J. Appl. Math.* **44**, 270–286 (1984)
9. Steindl, A., Troger, H.: Nonlinear three-dimensional oscillations of elastically constrained fluid conveying tubes with perfect broken $O(2)$ -symmetry. *Nonlinear Dyn.* **7**, 165–193 (1995)
10. Bajaj, A.K., Sethna, P.R.: Effect of symmetry-breaking perturbations on flow-induced oscillations in tubes. *J. Fluids Struct.* **5**, 651–679 (1991)
11. Yoshizawa, M., Suzuki, T., Hashimoto, K.: Nonlinear lateral vibration of a vertical fluid-conveying pipe with end mass. *JSME Int. J. Ser. C* **41**, 652–661 (1998)
12. Yamashita, K., Furuya, H., Yabuno, H., Yoshizawa, M.: Non-planar vibration of a vertical fluid-conveying pipe (effect of horizontal excitation at the upper end). *J. Vib. Acoust.* **136**, 041005-1–12 (2014)
13. Guckenheimer, G., Holmes, P.J.: *Nonlinear Oscillations, Dynamical Systems, and Bifurcations of Vector Fields*, pp. 396–398. Springer, New York (1983)

Publisher's Note Springer Nature remains neutral with regard to jurisdictional claims in published maps and institutional affiliations.